Collision spectroscopy of Ar^{8+} + He at low velocities ($v < 1$ a.u.)

S. Bliman,* M. G. Suraud, D. Hitz, and B. A. Huber
Département de Science des Matériaux, DRFG, Centre d' Etudes Nucléaires de Grenoble, Boîte Postale 85X, F-38041 Grenoble CEDEX, France

H. Lebius
Institut für Experimentalphysik AG II, Ruhr-Universität, D-4630 Bochum, Germany

M. Cornille
Departement d'Astronomie Relativiste et de Cosmologie, Observatoire de Paris, F-92195 Meudon CEDEX, France

J. E. Rubensson and J. Nordgren
Department of Physics, University of Uppsala, Box 530, S-7521 Uppsala, Sweden

E. J. Knystautas
Departement de Physique, Université Laval, Quebec, Canada G1K 7P4
(Received 21 January 1992)

Single- (SC) and double-electron capture (DC) have been studied for collisions of Ar^{8+} with He using x-ray and vacuum ultraviolet (vuv) spectroscopy at a collision energy of 80 keV as well as translational-energy spectroscopy (TES) at lower collision energies (8 keV). It is shown that both processes involving the ground-state ion terminate in vuv photon emission, i.e., nonautoionizing levels are populated. The SC, by the long-lived metastable species Ar^{8+*} $(2p^5 3s)^3P_{0,2}$, populates mostly the Na-like core-excited levels with $n=4$: Ar^{7+*} $(2p^5 3s\ ^3P\ 4l)^{2,4}L_J$. With the use of calculated decay and autoionization rates, the measured vuv spectra are analyzed and compared with the TES results and the Auger spectra measured by other authors. It is shown that the stabilization of these core-excited states is both radiative and autoionizing. The DC by the metastable projectile is not yet fully understood.

PACS number(s): 34.70.+e, 32.30.Jc, 32.90.+a

I. INTRODUCTION

Theoretical studies of charge-exchange collisions at low energies ($v < 1$ a.u.) have been performed for systems involving projectiles with closed shells (He- or Ne-like ions) and H and He targets. The main attention was focused on the single-electron-capture process. Only a limited number of calculations analyze the double-electron capture, even though the experimental effort has been largely developed [1,2].

Additional problems and difficulties arise from the fact that an ion beam may contain a metastable fraction, a situation which is frequently encountered in the experiment. In these cases, single-electron capture produces ions in doubly excited states, while double capture would end in triply excited states. These states share common features with those seen in dielectronic recombination processes.

The existence of ionic metastable states is very general in all quasi-two-electron systems. In the case of He-like ions, the metastable state $(1s2s)^3S_1$ is long lived ($\tau \geq 10^{-4}$ s for elements with a nuclear charge $Z < 10$) [3,4]; its decay into the ground state $1s^2\ ^1S_0$ occurs via a magnetic dipole transition ($M1$). For Be-like ions, the $1s^2 2s2p\ ^3P_{0,2}$ levels are long lived: the $^3P_0$ level could decay to the ground state via a two-photon transition $E1$-$M1$ and it is known that for low-Z ions this is very unlikely to occur. The $^3P_2$ decays to the ground state via a magnetic quadrupole transition ($M2$) and has a very small transition probability. The $^3P_1$ sublevel decays via an $E1$ transition.

For Ne-like ions, the existence of two spin states results in the occurrence of $2p^5 3s\ ^3P_{0,2}$ levels: they show characteristics basically similar to the $2s2p\ ^3P_{0,2}$ levels in Be-like ions. For Ne-like Ar, the lifetime of $2p^5 3s\ ^3P_{0.2}$ has been calculated ($\tau \sim 3.5 \times 10^{-4}$ s) and the L fluorescence of Na-like core-excited argon ions was observed following the single-electron capture by Ar^{8+} ions [5]. The spectroscopic observations were performed in the wavelength region below 5.5 nm where the normal Na-like Ar is not expected to give any emission line ($\lambda_{\text{limit}} = 8.64$ nm, ionization limit of Ar^{7+}). This gave evidence of a metastable content of the Ar^{8+} ion beam; a more detailed discussion of the metastable fraction will be given in the following experimental section.

Under these conditions, it was felt that the Ar^{8+} + He system had to be reconsidered for both single- and double-electron capture by both ion-core configurations. In Sec. II the experimental arrangements and methods are presented; Sec. III gives the experimental results, whereas Sec. IV outlines the general electron transfer features.

II. EXPERIMENTAL ARRANGEMENTS AND METHODS

The collision system $Ar^{8+}+He$ has been studied with two different experimental methods. On the one hand, the x-ray and vacuum ultraviolet (vuv) photon spectroscopy has been applied at a collision energy of 80 keV, yielding direct information on the decay of the populated excited states. On the other hand, the system has been studied with the aid of the translational-energy-spectroscopy (TES) technique at collision energies at 8 keV. This second method gives direct access to the states formed in the collision. In the following, we will give a brief description of both experimental arrangements.

A. X-ray and vuv spectroscopy

An Ar-ion beam delivered by the electron-cyclotron-resonance (ECR) ion source at the LAGRIPPA facility of the Centre d'Etudes Nucleaires de Grenoble is charge and mass analyzed in order to obtain a pure Ar^{8+} beam. The typical ion current is 5 μA at 80 keV, the ion velocity amounts to 0.28 a.u. The ion beam is passed into a collision chamber where the target gas (He) pressure is kept at about 4×10^{-3} Pa (measured with a Baratron). The collision chamber is pumped differentially allowing a background pressure of about 10^{-5} Pa. In this situation the single-collision condition is met.

Following electron capture into excited states of Ar^{7+} and Ar^{6+}, the subsequent spontaneously emitted photons are analyzed with a 1-m grazing-incidence (85°) vuv grating (1200 lines/mm) monochromator and are detected with a channel electron multiplier. The entrance slit (width of 400 μm) is located 53 cm apart from the scattering center, admitting photons, which are emitted at 25° with respect to the forward beam direction. Photons emerging from the exit slit (width of 400 μm) are analyzed in wavelength by displacing the detector. The intensity calibration of the spectrometer was determined by the branching-ratio method [6]. Each channel in the measured spectra represents approximatively a spectral region of 0.1 nm, the scanning speed was 20–30 s per channel. Figure 1 shows a survey spectrum normalized in intensity where the photon detection efficiency as a function of the wavelength has been accounted for. Figure 2 gives the intensity-calibration curve of the spectrometer.

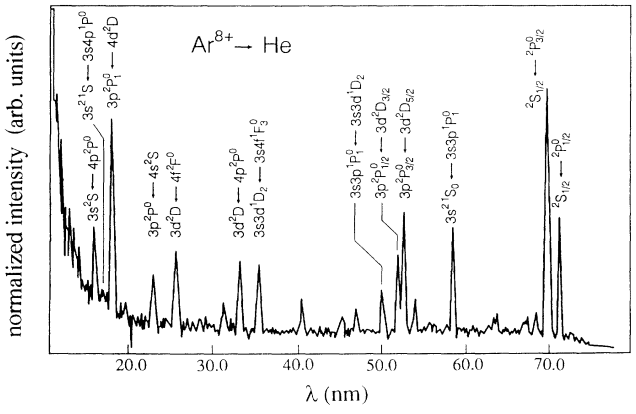

FIG. 1. Normalized intensity survey spectrum for $Ar^{8+}+He$ at 2 keV/u.

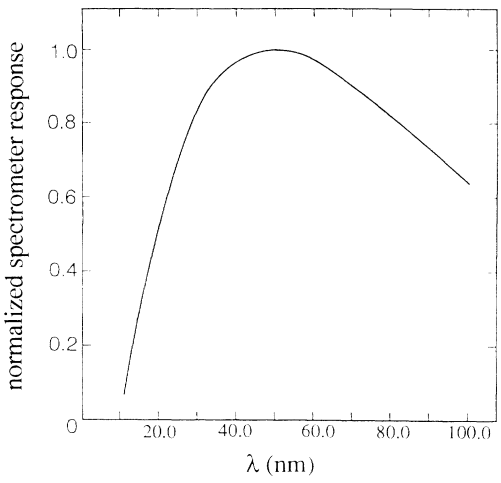

FIG. 2. Intensity calibration curve of the vuv monochromator.

Figure 3 represents the soft x-ray spectrum in the wavelength range below 5.5 nm easily interpreted as resulting from single-electron capture by the metastable Ar^{8+} ion [5]. This spectrum has been recorded with a grazing-incidence spectrometer looking at 90° to the beam direction. A 3-m grating with 300 lines/mm was used [7] and a 68-μm entrance slit was chosen. The detector consisted of a multichannel plate device with a resistive-anode readout technique. The detection efficiency was enhanced by a CsI coating of the detector and by using an electron-capturing electric field provided by a grid mounted over the detector surface. The wavelength scale has been calibrated by well-known emission lines [8] as shown in Fig. 4. Single-electron capture has been studied for $Ar^{9+}+He$ collisions and the observed two strong lines are identified as the cascade termination: $2p^5 3s\ ^1P_1^\circ \rightarrow 2p^6\ ^1S_0$ at 4.873 nm and $2p^5 3s\ ^3P_1^\circ \rightarrow 2p^6\ ^1S_0$ at 4.918 nm. These lines served as reference wavelengths for the analysis of the lines shown in Fig. 3.

B. Translational-energy spectroscopy

The principle of the applied method as well as details on the experimental setup are given in previous publications [9,10]. Therefore only a brief description will be given here. The beam of multiply charged ions is delivered by the "LAGRIPPA" facility at a collision energy of 1 keV per charge. In order to narrow the energy distribution of the primary beam, the ions pass an energy monochromator, yielding an energy profile with a half width at half maximum smaller than 0.5 eV per charge. Secondary ions are detected at different scattering angles; they are analyzed with respect to their charge state and their kinetic energy by the aid of a second energy analyzer. From an analysis of the energy gain of the projectiles, the excitation energy and hence the final-state population can be determined.

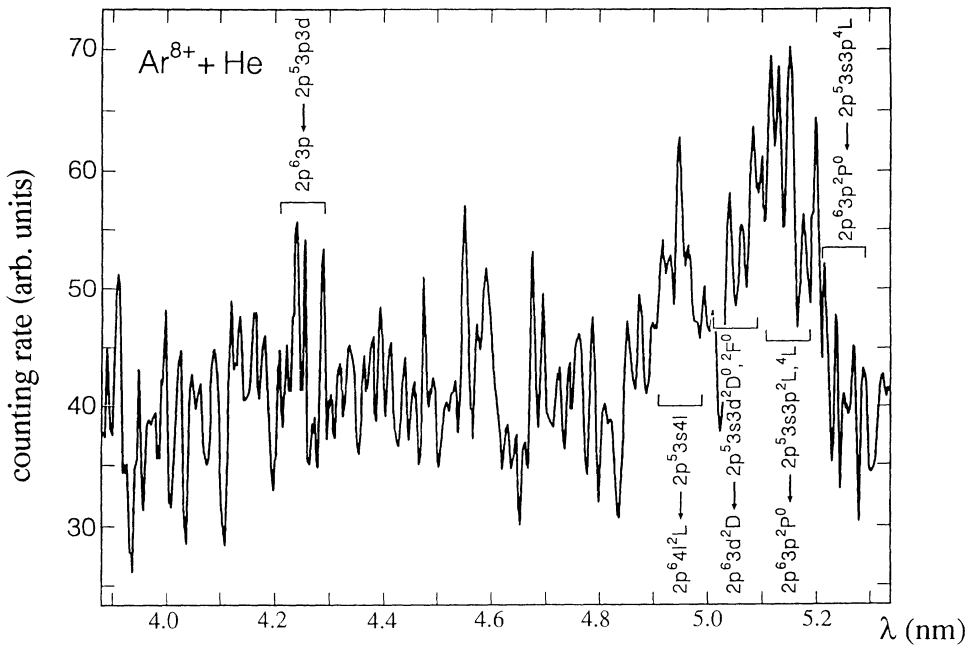

FIG. 3. Normalized intensity soft x-ray spectrum for $Ar^{8+*}(2p^5 3s)^3P^{\circ}_{0,2}$ + He at 2 keV/u.

In the case of Ar^{8+} the metastable fraction of the ion beam was found to be very narrow (<5%). In order to increase this metastable fraction, a state-preparing electron-capture reaction has been applied in the beam line of LAGRIPPA between the two mass-to-charge-ratio analyzing magnets. Whereas the first magnet was set for a transmission of Ar^{9+} ions, the second one could be passed only by Ar ions in charge state 8, being produced in a gas target in between. The corresponding electron-capture reaction is described as follows:

$$Ar^{9+}(2p^5)+X \rightarrow Ar^{8+*}[2p^5(4l,5l)]+X^+ , \quad (1)$$

with X = He, N_2, and air.

The Ar^{8+} ions which are produced in the excited levels $n=4,5$ will decay during their flight time (60 μs) before reaching the collision chamber and a large fraction of these ions will end up in the metastable levels $(2p^5 3s)^3P_{0,2}$.

As mentioned before, single-electron capture by metastable excited Ar^{8+} projectiles results in the formation of doubly excited states which may decay via autoionization. The resulting Ar^{8+} ions which have gained energy in the capture process are used as indicator for the metastable species. Figure 5 shows the energy distribution of these ions using an unprepared ion beam as well as an ion beam, which has been prepared according to reaction (1)

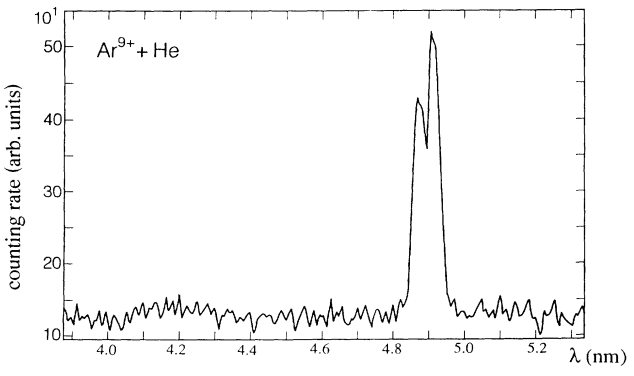

FIG. 4. Normalized intensity soft x-ray spectrum for $Ar^{9+}(2p^5)+He \rightarrow Ar^{8+}(2p^5 nl)^{1,3}L+He^+$; near 4.9 nm, the peaks correspond to $2p^5 3s\ ^1P^{\circ}_1 \rightarrow 2p^6\ ^1S_0$ (4.873 nm) and $2p^5 3s\ ^3P_1{}^{\circ} \rightarrow 2p^6\ ^1S_0$ (4.918 nm).

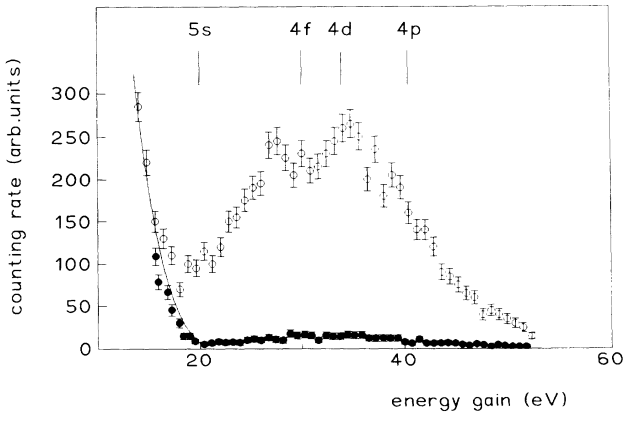

FIG. 5. Energy distribution of Ar^{8+} ions produced by single-electron capture in $Ar^{8+*}(2p^5 3s)^3P_{0,2}$ + He collisions followed by autoionization. Full dots: Ar^{8+} beam extracted directly from the ECR ion source; open circles: Ar^{8+} beam prepared in Ar^{9+} + air collisions.

with X=air. Both curves are normalized to the same primary ion current and target thickness in the collision chamber. In the case of the state-prepared ion beam, the metastable fraction is found to be increased by a factor of about 15. From an analysis of the translational-energy spectra, which are discussed below and which are obtained for both types of beams, absolute values of the metastable fractions are estimated, yielding 45% and 3%, respectively. (The evaluation method, within which equal single-capture cross sections are assumed for both projectile states, is described in more detail in Ref. [11].) If nitrogen is used in reaction (1) as a target gas, the effect is found to be similar; however, in the case of He the measured increase of the metastable fraction is a factor of 5 only. This is due to the fact that in this case lower excited levels of the Ar^{8+} projectiles are populated.

III. ANALYSIS OF THE MEASURED SPECTRA

In the following the vuv spectra obtained at a collision energy of 80 keV and the translational-energy spectra measured at 8 keV will be discussed.

A. X-ray and vuv spectra

In view of the complex situation resulting from the different possible mechanisms ending in the population of excited levels, namely,

$$Ar^{8+}(2p^6)^1S_0+He\rightarrow Ar^{7+*}(nl)^2L_j+He^+ , \quad (2)$$

$$Ar^{8+}(2p^6)^1S_0+He\rightarrow Ar^{6+**}(nl,n'l')^1L_J+He^{2+} , \quad (3)$$

$$Ar^{8+*}(2p^5 3s)^3P_{0,2}+He \rightarrow Ar^{7+**}[(2p^3 3l)^3Ln'l']^{2,4}L_J+He^+ , \quad (4)$$

we consider separately the radiative pattern following each transfer process.

1. Normal Na-like spectrum

With the combined use of known data [8,12,13] the Na-like argon transitions were identified. They are shown in Table I with their normalized intensities. They are unambiguously attributed to the radiative decay following single-electron capture (reaction 2).

TABLE I. Na-like Ar transitions following the capture collisions: $Ar^{8+}(2p^6)^1S_0+He\rightarrow Ar^{7+}(nl)^2L+He^+$. Each transition is given with its wavelength and normalized intensity.

Transition	λ (nm)	Intensity
$4p\ ^2P^\circ\rightarrow 3s\ ^2S_{1/2}$	15.9	43
$4p\ ^2P^\circ\rightarrow 3d\ ^2D$	33.8	30
$4s\ ^2S_{1/2}\rightarrow 3p\ ^2P^\circ$	23.1	23
$4f\ ^2F^\circ\rightarrow 3d\ ^2D$	26.03	34
$4d\ ^2D\rightarrow 3p\ ^2P^\circ$	18.0	90
$3d\ ^2D_{3/2}\rightarrow 3p\ ^2P^\circ_{1/2}$	51.94	35
$3d\ ^2D_{5/2}\rightarrow 3p\ ^2P^\circ_{3/2}$	52.67	54
$3p\ ^2P^\circ_{3/2}\rightarrow 3s\ ^2S_{1/2}$	70.025	108
$3p\ ^2P^\circ_{1/2}\rightarrow 3s\ ^2S_{1/2}$	71.38	54

From the consideration of the line intensities, we note that (1) the experimental $4p\ ^2P_0$ intensity ratio for the decay to both $3s\ ^2S_{1/2}$ and $3d\ ^2D_J$, $R_{expt}=I(4p\rightarrow 3s)/I(4p\rightarrow 3d)=1.43$, which compares well with the calculated value $R_{theor}=1.33$ [13]; (2) the intensity ratio $R=I(3d\ ^2D_{5/2}\rightarrow 3p\ ^2P^\circ_{3/2})/I(3d\ ^2D_{3/2}\rightarrow 3p\ ^2P^\circ_{1/2})$ is normally estimated to be 2 while the experiment gives the value of 1.55; and (3) the intensity ratio $R=I(3p\ ^2P^\circ_{3/2}\rightarrow 3s\ ^2S_{1/2})/I(3p\ ^2P^\circ_{1/2}\rightarrow 3s\ ^2S_{1/2})$ is equal to 2 as expected theoretically. Given the intensity-calibration uncertainty, mostly in the wavelength range below 50 nm, we conclude that the sharing among the $n=4$ sublevels is not statistical in L but in each L the sharing in J is statistical.

2. Mg-like Ar transitions

In the case of process (3), taking into account Wigner's spin conservation rule, it is expected that the double-electron capture should populate singlet states in the Mg-like Ar spectrum. For the line identification, use was made of known data [8,12] and of recently calculated and measured wavelengths [14–16]. Table II gives the identified transitions with their wavelength and normalized intensity. It should be noted that the populated levels need be of even parity. Therefore the dominant part from the measured line emission results from cascades from the captured levels, i.e., is attributed to the direct double-electron capture followed immediately by cascade processes.

3. Core-excited Na-like Ar transitions

As has been observed in other systems involving single-electron capture by a metastable ion [3,4]—for example, capture by He-like ions will end in Li-like core-excited $^{2,4}L_J$ levels—the ^4L_J levels are in general metastable against autoionization and thus cascade radiatively down to the lowest-lying ^4L_J levels. For Li-like ions, the lowest levels are $1s2s2p\ ^4P_{1/2,3/2,5/2}$ which in turn may share their stabilization between radiation and autoionization.

For Ne-like argon, it has been shown [5] that the long-lived metastable levels $Ar^{8+*}(2p^5 3s)^3P_{0,2}$ may capture one electron and thus populate core-excited Na-like levels fluorescing in the soft x-ray range below 5.5 nm (see Figs. 1 and 3).

For the purpose of identifying the ^4L to ^4L transitions, likely to be in the vuv spectrum, as well as the ^2L to ^2L

TABLE II. Mg-like Ar transitions following double-electron capture $Ar^{8+}(2p^6)^1S_0+He\rightarrow Ar^{6+}(nl,n'l')^1L+He^+$.

Transition	λ (nm)	Intensity
$3s4s\ ^1S_0\rightarrow 3s3p\ ^1P^\circ_1$	28.14	5
$3s4p\ ^1P^\circ_1\rightarrow 3s^2\ ^1S_0$	17.54	8
$3s4d\ ^1D_2\rightarrow 3s3p\ ^1P^\circ_1$	21.56	7
$3s4f\ ^1F^\circ_3\rightarrow 3s3d\ ^1D_2$	35.05	25
$3s3d\ ^1D_2\rightarrow 3s3p\ ^1P^\circ_1$	50.01	12
$3s3p\ ^1P^\circ_1\rightarrow 3s^2\ ^1S_0$	58.53	48

transitions, several calculations have been performed yielding energies, autoionization probabilities and transition probabilities for the $(2p^5 3sn'l')^{2,4}L_J$ levels with $n'=3,4$. The SUPERSTRUCTURE code [17] gives wavelengths and transition probabilities, the DISTORTEDWAVE code [18,19] gives autoionization probabilities in *LS* coupling, whereas the AUTOLSJ code [20] gives the Auger rates in *LSJ* coupling. The results of these calculations are presented in Tables III–V. In Table III the $(2p^5 3l3l')^{2,4}L_J$ levels are tabulated, complementing

TABLE III. Theoretical data for $Ar^{7+}(2p^5 3l3l')$ $(l,l'=1,2)$. First column: level designation; second column: energies from ground state $3s\ ^2S_{1/2}$ (in eV); third column: autoionization probabilities; fourth column: sum of transition probabilities; fifth column: total fluorescence yield. The numbers in brackets in the third through fifth columns indicate the multiplicative power of ten.

Level	Energy (eV)	A_a	$\sum_r A_r$	ω_T
$2p^5 3p^2\ ^2P^\circ_{1/2}$	273.60	2.02[+13]	5.75[+10]	3[−03]
$^2P^\circ_{3/2}$	273.92	1.62[+13]	3.99[+10]	2[−03]
$^2F^\circ_{7/2}$	274.44	4.31[+10]	1.52[+10]	0.26
$^2F^\circ_{5/2}$	275.52	2.43[+10]	1.25[+10]	0.34
$^2D^\circ_{5/2}$	277.36	1.37[+10]	8.58[+09]	0.39
$^2D^\circ_{3/2}$	277.60	2.12[+12]	8.16[+09]	4[−03]
$2p^5 3p3d\ ^2D_{5/2}$	297.69	1.91[+11]	1.81[+10]	0.09
$^2D_{3/2}$	297.94	1.97[+11]	4.52[+10]	0.19
$^2P_{1/2}$	298.70	1.76[+07]	8.48[+10]	1
$^2F_{5/2}$	299.88	3.62[+10]	1.27[+10]	0.26
$^2P_{3/2}$	300.40	1.89[+09]	1.31[+10]	0.87
$^2S_{1/2}$	306.25	7.03[+12]	3.42[+11]	0.05
$2p^5 3d^2\ ^2G^\circ_{7/2}$	325.20	1.86[+11]	1.58[+10]	0.08
$^2F^\circ_{5/2}$	326.26	3.34[+13]	5.57[+10]	2[−03]
$^2F^\circ_{7/2}$	326.30	1.45[+13]	1.46[+10]	1[−03]
$^2D^\circ_{5/2}$	326.65	3.32[+12]	6.21[+10]	0.02
$^2D^\circ_{3/2}$	326.87	6.84[+11]	3.97[+10]	0.05
$^2P^\circ_{1/2}$	327.17	1.22[+12]	2.20[+10]	0.02
$^2P^\circ_{3/2}$	328.36	1.43[+11]	7.43[+10]	0.34
$2p^5 3p^2\ ^4P^\circ_{5/2}$	275.73	1.41[+08]	5.90[+09]	0.98
$^4P^\circ_{3/2}$	274.80	3.48[+12]	1.61[+10]	5[−03]
$^4P^\circ_{1/2}$	275.11	8.69[+11]	9.04[+09]	0.01
$^4D^\circ_{7/2}$	275.82	4.80[+06]	6.61[+09]	1
$^4D^\circ_{5/2}$	276.14	4.07[+08]	6.67[+09]	0.94
$^4D^\circ_{3/2}$	276.38	9.55[+10]	5.76[+09]	0.06
$^4D^\circ_{1/2}$	277.36	2.44[+11]	8.22[+09]	0.03
$^4S^\circ_{1/2}$	279.11	6.44[+11]	9.39[+09]	0.01
$2p^5 3p3d\ ^4D_{1/2}$	294.97	6.71[+05]	1.30[+09]	1
$^4D_{3/2}$	295.19	7.79[+09]	3.21[+09]	0.29
$^4D_{5/2}$	295.50	1.42[+10]	4.57[+09]	0.24
$^4G_{5/2}$	297.56	6.18[+10]	7.22[+09]	0.10
$^4F_{3/2}$	299.80	1.64[+11]	6.02[+10]	0.27
$^4S_{3/2}$	300.09	1.16[+10]	1.58[+10]	0.58
$^4F_{5/2}$	300.19	5.86[+10]	1.77[+10]	0.23
$^4P_{1/2}$	300.32	2.39[+11]	2.41[+10]	0.09
$^4P_{5/2}$	300.51	2.18[+10]	1.30[+10]	0.37
$^4P_{3/2}$	300.73	1.67[+07]	2.30[+10]	1
$2p^5 3d^2\ ^4D^\circ_{1/2}$	323.01	9.46[+08]	1.47[+10]	0.94
$^4D^\circ_{3/2}$	323.11	1.14[+09]	1.58[+10]	0.93
$^4D^\circ_{5/2}$	323.27	4.88[+09]	1.69[+10]	0.78
$^4D^\circ_{7/2}$	323.54	1.35[+11]	1.84[+10]	0.12
$^4G^\circ_{7/2}$	324.43	4.97[+10]	1.92[+10]	0.28
$^4G^\circ_{5/2}$	324.72	7.50[+11]	2.16[+10]	0.03
$^4F^\circ_{3/2}$	325.41	3.05[+10]	9.14[+10]	0.75
$^4P^\circ_{5/2}$	325.57	2.56[+11]	2.94[+11]	0.10
$^4F^\circ_{5/2}$	325.73	1.46[+12]	6.84[+10]	0.04
$^4P^\circ_{3/2}$	326.03	3.84[+08]	2.57[+10]	0.95
$^4P^\circ_{1/2}$	326.40	6.17[+09]	2.21[+10]	0.78
$^4F^\circ_{7/2}$	326.82	2.04[+13]	3.20[+10]	2[−03]
$^4S^\circ_{3/2}$	330.51	7.94[+11]	7.78[+10]	0.09

TABLE IV. Theoretical data for $Ar^{7+}(2p^5 3s4l)^4L$ (see caption of Table III).

Level	Energy (eV)	A_a	$\sum_r A_r$	ω_T
$2p^5 3s4s\ ^4P^\circ_{5/2}$	315.65			
$^4P^\circ_{3/2}$	316.29	1.19[+10]	3.20[+10]	0.73
$^4P^\circ_{1/2}$	318.33	1.62[+10]	6.18[+10]	0.79
$2p^5 3s4p\ ^4S_{3/2}$	322.17	1.0[+05]	4.31[+08]	0.99
$^4D_{7/2}$	322.73		5.71[+08]	1
$^4D_{5/2}$	322.89	2.84[+08]	5.66[+08]	0.67
$^4D_{3/2}$	323.24	6.72[+08]	5.39[+08]	0.45
$^4P_{5/2}$	323.48	8.31[+08]	5.96[+08]	0.42
$^4D_{1/2}$	323.64	3.61[+11]	5.71[+08]	2[−03]
$^4P_{1/2}$	324.80	7.93[+12]	6.19+08]	<1[−03]
$^4P_{3/2}$	325.41	2.07[+09]	5.75[+08]	0.22
$2p^5 3s4d\ ^4P^\circ_{1/2}$	331.01	1.98[+09]	2.34[+09]	0.54
$^4P^\circ_{3/2}$	331.18	8.06[+09]	4.81[+09]	0.37
$^4F^\circ_{9/2}$	331.36		1.29[+09]	1
$^4P^\circ_{5/2}$	331.46	1.03[+09]	1.31[+09]	0.56
$^4F^\circ_{7/2}$	331.58	9.61[+10]	1.34[+09]	0.01
$^4F^\circ_{5/2}$	331.87	1.09[+11]	1.32[+09]	0.01
$^4F^\circ_{3/2}$	332.17	1.20[+11]	2.52[+10]	0.02
$^4D^\circ_{7/2}$	332.61	5.14[+11]	1.26[+09]	0.002
$^4D^\circ_{1/2}$	332.92	1.20[+12]	2.98[+11]	0.20
$^4D^\circ_{3/2}$	333.34	6.57[+11]	1.89[+11]	0.22
$^4D^\circ_{5/2}$	334.04	3.13[+11]	1.31[+09]	4[−03]
$2p^5 3s4f\ ^4D_{1/2}$	334.98	7.70[+03]	9.11[+07]	0.999
$^4D_{3/2}$	335.04	2.59[+09]	8.75[+07]	0.03
$^4G_{11/2}$	335.10		7.78[+07]	1
$^4D_{5/2}$	335.13	2.41[+09]	8.21[+07]	0.03
$^4G_{9/2}$	335.23	3.27[+09]	7.32[+07]	0.18
$^4F_{7/2}$	335.26	4.64[+08]	7.40[+07]	0.14
$^4G_{7/2}$	335.55	2.00[+09]	7.60[+07]	0.04
$^4F_{9/2}$	335.60	4.34[+09]	6.50[+07]	0.02
$^4F_{5/2}$	335.60	9.29[+10]	5.70[+07]	6[−04]
$^4F_{3/2}$	335.61	2.86[+11]	3.71[+09]	1[−04]
$^4D_{7/2}$	337.61	5.35[+09]	7.09[+07]	0.01
$^4G_{5/2}$	337.61	4.08[+10]	6.58[+06]	2[−03]

TABLE V. Theoretical data for $Ar^{7+}(2p^5 3s4l)^2L$ (see caption of Table III).

Level	Energy (eV)	A_a	$\sum_r A_r$	ω_T
$2p^5 3s4s\ ^2P^\circ_{1/2}$	316.94	2.05[+09]	6.23[+10]	0.97
$^2P^\circ_{3/2}$	318.26	1.54[+12]	8.58[+10]	0.05
$2p^5 3s4p\ ^2S_{1/2}$	323.88	4.96[+12]	3.44[+08]	<1[−04]
$^2D_{3/2}$	323.98	5.58[+09]	5.44[+08]	0.09
$^2D_{5/2}$	324.22	4.30[+09]	3.77[+08]	0.08
$^2P_{3/2}$	324.41	3.36[+07]	3.92[+08]	0.92
$^2P_{1/2}$	325.52	6.86[+12]	4.94[+08]	<1[−04]
$2p^5 3s4d\ ^2F^\circ_{7/2}$	332.05	1.01[+12]	1.24[+09]	0.001
$^2P^\circ_{1/2}$	332.46	4.32[+11]	3.73[+10]	0.08
$^2P^\circ_{3/2}$	332.59	1.19[+11]	4.84[+09]	0.04
$^2D^\circ_{5/2}$	332.70	1.65[+10]	1.29[+09]	0.07
$^2F^\circ_{5/2}$	332.73	5.67[+11]	1.26[+09]	2[−03]
$^2D^\circ_{3/2}$	334.33	5.92[+11]	1.17[+11]	0.16
$2p^5 3s4f\ ^2G_{7/2}$	336.14	9.65[+10]	6.21[+07]	6[−04]
$^2D_{5/2}$	336.16	5.05[+10]	4.75[+07]	1[−03]
$^2D_{3/2}$	336.53	8.66[+11]	9.30[+07]	5[−04]
$^2G_{9/2}$	336.57	8.72[+11]	9.63[+07]	5[−04]
$^2F_{7/2}$	336.67	2.63[+11]	9.45[+07]	5[−04]
$^2F_{5/2}$	338.55	1.82[+11]	8.11[+07]	4[−04]

Tables 1 and 2 of a previous paper [5], where all $2p^5 3s 3p$ and $2p^5 3s 3d$ levels have been given. Table IV contains the data for the $(2p^5 3s 4l)^4L_J$ levels and Table V for the corresponding ^2L_J levels. Each level is characterized by its energy from the ground state $2p^6 3s\ ^2S_{1/2}$ (in eV), the Auger transition probability A_a, the sum of the transition probabilities $\sum_r A_r$ and its total fluorescence yield defined as $\omega_T = \sum_r A_r / [(\sum_r A_r) + A_a]$.

Considering these results, two remarkable features are evidenced: For many levels a J-dependent differential metastability is clearly seen. As was observed in the Mg-like Ar radiative decay, there are channels where two-electron–one-photon transitions are possible, starting from the upper configurations $2p^6 3s 4l$ [14]. This justifies the calculation of $2p^5 3p^2$, $2p^5 3p 3d$, and $2p^5 3d^2$ configurations with $2p^5 3p\ ^3L$ cores. The overall level diagrams for doublets and quartets are shown in Figs. 6 and 7.

The radiative and nonradiative decay of doubly excited configurations in the Ar^{7+} spectrum has been discussed also in a recent paper [21]; however, as only configuration-averaged values are given, a detailed comparison with our presented values cannot be made.

In Fig. 4 the most important decay channels as identified with our calculations are shown. The ion time of flight in front of the spectrometer entrance is of the order of 3.2×10^{-8} s. This time is by far longer than the lifetime of any of the populated levels (either directly or through cascades). The spectrum of Fig. 1 shows some weak-intensity lines which are attributed to cascade transitions among quartet states. A tentative assignment of these lines is given in Table VI.

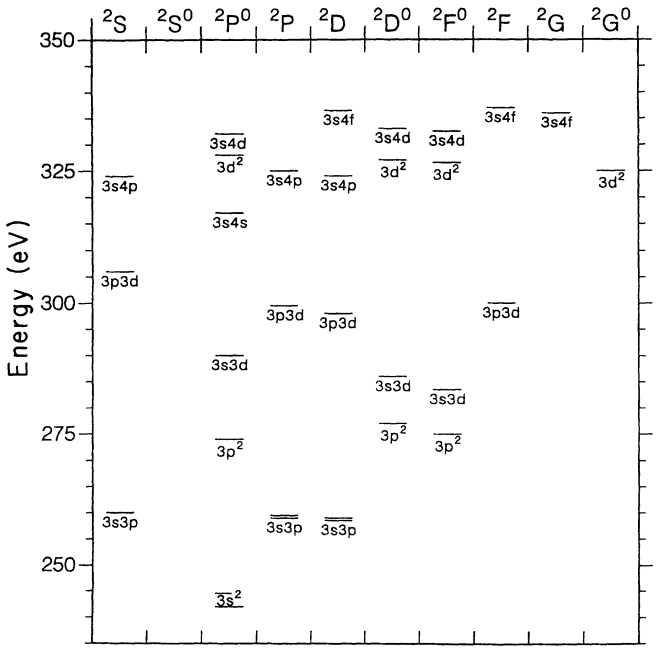

FIG. 6. Grotrian diagram for $Ar^{7+}(2p^5 3l n'l')^2L$ with $l=0,1,2$ for $n'=3$ and $l'=0.1,2$; for $n'=4, l=0$ and $l'=0,1,2,3$. Energies are given in eV above the ground level; the ionization energy of Ar^{7+} is 143.456 eV.

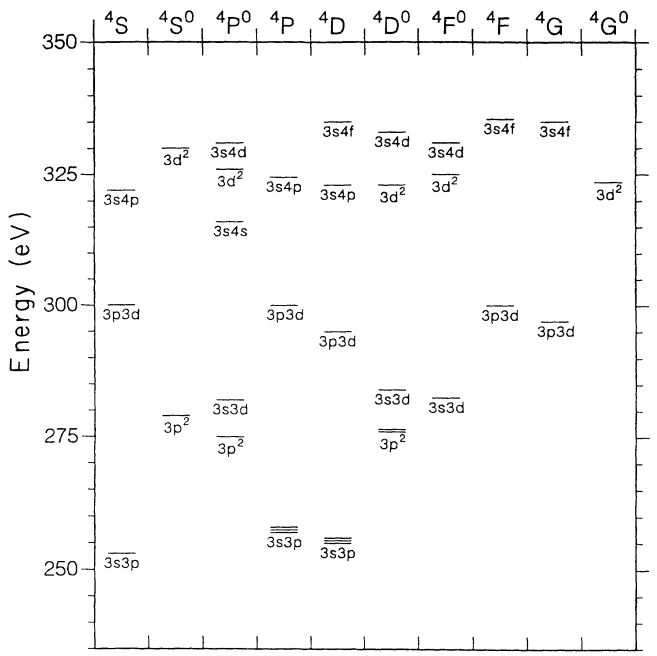

FIG. 7. Grotrian diagram for $Ar^{7+}(2p^5 3l n'l')^4L$ (see caption Fig. 6).

Under the same experimental conditions Mack [22] recorded an Auger electron spectrum where no peak identification has been suggested. Even though complex, it is possible to identify some of the Auger lines (see Table VI). For the Auger decay only the $2p^6\ ^1S_0$ continuum is available. If the measured line positions are compared

TABLE VI. Optical transitions and Auger lines with tentative assignment.

Optical transitions	
Wavelengths (nm)	Assignments
68.0	$3s3d\ ^4F^\circ \rightleftharpoons 3p3d\ ^4F$
63.0	$3p^2\ ^4P^\circ \rightleftharpoons 3p3d\ ^4D$
62.7	$3p^2\ ^4P^\circ \rightleftharpoons 3p3d\ ^4D$
60.7	$3p^2\ ^4S^0 \rightleftharpoons 3p3d\ ^4P$
53.7	$3p^2\ ^4D^0 \rightleftharpoons 3p3d\ ^4F$
46.6	$3s3p\ ^4D \rightleftharpoons 3s3d\ ^4F^\circ$
44.8	Unidentified
40.2	Unidentified
31.7	Unidentified
19.8	$3s3p\ ^4S \rightleftharpoons 3s4s\ ^4P^\circ$

Auger lines			
Energy (eV)	Intensity	Assignment	Calc. (eV)
245	medium	$2p^5 3s^2\ ^2P_{3/2}$	242
247	medium	$2p^5 3s^2\ ^2P_{1/2}$	244
278	weak	$3s3d\ ^4P$	282
297	weak	$3p3d\ ^2F,\ ^2D$	300
320	medium	$3s4s\ ^2P$	318
326–328	intense	$3s4p\ ^2L$	324–325
334	intense	$3s4d\ ^2L$	330–332
337	medium	$3s4f\ ^2L,\ ^4L$	336

with the calculated energy levels, a good agreement is found; however, a systematic shift of the order of 2 eV is noted between the measured and the calculated values. Another important conclusion can be drawn: the intensity ratio of the lines originating from $2p^5 3s^2\,{}^2P_{3/2}$ and $2p^5 3s^2\,{}^2P_{1/2}$ is 2, showing that the J sharing is statistical. The line identification shows two different groups: the most intense and unresolved is unambiguously attributed to $2p^5 3s 4l\,{}^{2,4}L$ states; a group of low-intensity lines appears to result from cascades initiated at $3s4l$ levels through either two-electron and/or one-electron transitions. The $2p^5 3s^2\,{}^2P^0_{3/2,1/2}$ lines are the end of the cascades among these doubly excited ^2L levels. The ^4L levels share their stabilization between radiation and autoionization (see also discussion below), cascading down to the lowest-lying core-excited level $2p^5 3s 3p\,{}^4S_{3/2}$. A typical cascade time scale as appears from Tables III and IV is of the order of 10^{-11}–10^{-13} s (level lifetime). At the given ion velocity, the flight distance while cascading is less then 6×10^{-4} cm.

B. Translational-energy spectra

1. *Single-electron capture by* $Ar^{8+}(2p^6)^1S_0$

In order to study single-electron capture by Ar^{8+} ions in their electronic ground state, an ion beam extracted directly from the ECR ion source has been used. In this case, the majority of the projectiles (about 95%) are present in the ground state and, therefore, the dominant structures measured in the energy-gain spectra are attributed to $Ar^{8+}(2p^6)^1S_0$.

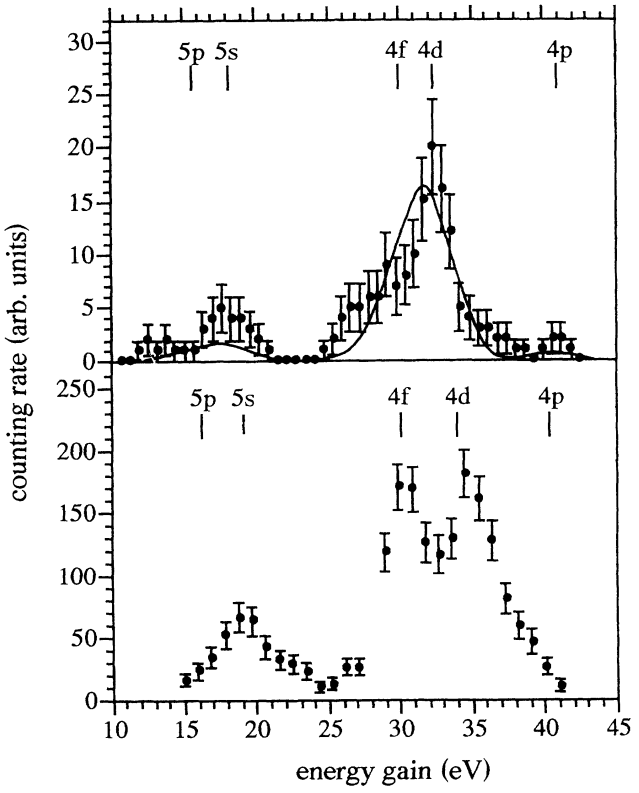

FIG. 8. Energy-gain spectra for Ar^{7+} ions produced in Ar^{8+}+/He collisions at $E=8.1$ keV and $\Theta=0°$. Upper part: ground-state projectiles $Ar^{8+}(2p^6\,{}^1S_0)$; lower part: metastable excited projectiles $Ar^{8+*}(2p^5 3s)^3P_{0,2}$.

TABLE VII. Relative population of excited Ar^{7+*} states after single-electron capture: $Ar^{8+}(2p^6)^1S_0$+He. Collision energy: 8.1 keV.

4*s*	4*p*	4*d*	4*f*	5*s*	Reference
	4	56	34	6	present (expt.)
	3	57	29	7	present (MCLZ)
9	31	41	19		Ref. [23] (expt.)
	7	55	38		Ref. [23] (theory)
	11	61	28		Ref. [24] (theory)
	2	90		8	Ref. [25] (expt.)

Figure 8 (upper part) shows the energy distribution of the corresponding Ar^{7+*} ions, produced at a scattering angle of 0° and a collision energy of 8100 eV. The bars at the top of the spectrum indicate those energy gains which characterize capture into specific *nl* configurations. Single-electron capture occurs dominantly into the 4*d* orbital; with somewhat lower probability the orbitals 4*p*, 4*f*, and 5*s* are populated. The full curve in the figure represents the result of a multichannel-Landau-Zener calculation (MCLZ) integrated over all scattering angles and convoluted with the energetic resolution of the spectrometer.

In order to facilitate a comparison with the results of other authors, the relative populations of the excited Ar^{7+} states are given in Table VII. Generally, good agreement is found with existing theoretical predictions [23,24] and experimental results [25]; however, the vuv studies of Druetta *et al.* [23] and earlier calculations of Kimura and Olson [26] result in a stronger population of the 4*p* level or the 4*f* level, respectively.

2. *Single-electron capture by excited* $Ar^{8+*}(2p^5 3s)^3P_{0,2}$

Electron capture by the metastable excited projectile has been studied with an enriched ion beam (see discussion above). Nevertheless, it was necessary to apply a subtraction procedure to obtain a pure "metastable" spectrum. For this purpose the measured spectrum had been corrected by the spectrum shown in the upper part of Fig. 8; the absolute amount of the ground-state contribution was determined by two requirements: On the one hand, the resulting difference spectrum had to stay positive in the total energy range; on the other hand, the width of the resulting structures had to be in agreement with the experimental resolution. The spectrum which has been obtained in this way is shown in the lower part of Fig. 8.

Single-electron capture by the metastable projectile is found to produce exclusively the configurations $2p^5 3snl$. However, as the ions are analyzed in charge state 7, the spectrum shown contains only contributions from those doubly excited Ar^{7+} states which are metastable with respect to autoionization and which stabilize radiatively. As in the case of the ground-state species, capture occurs

dominantly into states with $n=4$. The vertical bars indicate the energetic positions of the averaged configurations $2p^5 3snl$, as being calculated with a multiconfiguration Dirac-Fock code [27]. Besides the $4d$ and $4f$ orbitals, the $5s$ orbital is populated to a remarkable amount.

The general similarity between both spectra is due to the fact that the relative excitation energies of the considered levels are not very different with respect to the $2p^6$ and the $2p^5 3s$ ion cores. Hence the energy gain is very similar in both cases. Obviously, the excited $3s$ electron does not have a large influence on the electron-capture process.

The energy-gain spectrum of those ions which are populated in autoionizing states has already been shown in Fig. 5. Due to the kinematic broadening by the electron emission the spectrum is less well resolved; however, the measured energy gains are comparable with those shown in the lower part of Fig. 8 and therefore we may conclude that similar doubly excited states are populated. A slight shift towards lower-energy defects, which corresponds to larger excitation energies of the produced states, may be due to the fact that dominantly the doublet levels $2p^5 3snl\ ^2L_J$ are contributing to the autoionization signal.

A quantitative comparison of the different spectra yields an estimate for the fraction of doubly excited levels which decay by autoionization. The analysis shows that 54% of the reaction products stabilize by photon emission, whereas 46% decay via autoionization. If doublet and quartet levels are populated according to their statistical weights and if the LS-coupling scheme holds rigorously, an autoionizing fraction of 33% should be expected. This demonstrates that also quartet levels decay partially by autoionization in agreement with the calculated Auger rates.

3. *Double-electron capture by* $Ar^{8+}(2p^6)^1S_0$

The energy-gain spectrum of Ar^{6+} ions which are produced by true (nonautoionizing) double-electron capture is shown in Fig. 9. The prominent reaction channels lead to the formation of the $2p^6 3d4f$ and the $2p^6 3d4d$ Mg-

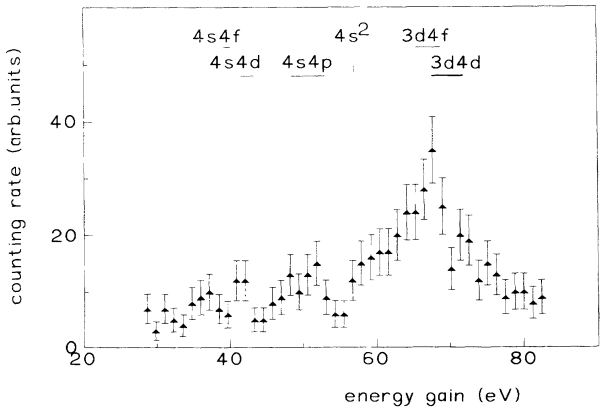

FIG. 9. Energy-gain spectrum of Ar^{6+} ions produced in $Ar^{8+}(2p^6)^1S_0$+He collisions. Scattering angle 0°; energy 8.1 keV.

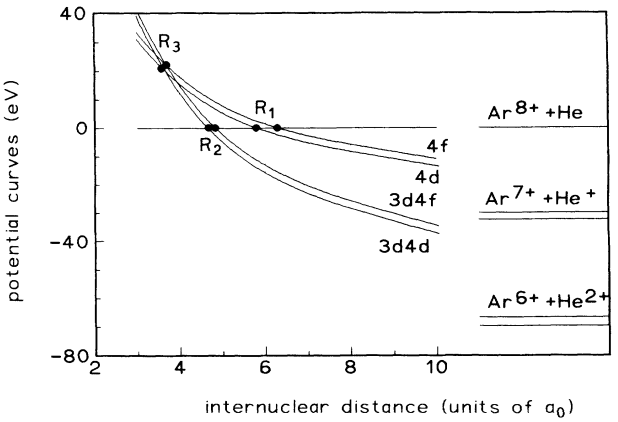

FIG. 10. Schematic potential-energy diagram representing the dominant single- and double-electron-capture channels.

like configurations, which are lying just below the autoionization limit. The $4s4l$ configurations which are above the ionization limit are populated to a minor extent only. The corresponding autoionizing signal can be seen in the energy-gain spectrum of Ar^{7+} ions measured at larger scattering angles (about 0.4°). A population of the $3p4l$ and $3s4l$ configurations has not been detected. The corresponding reaction probability is expected to be very small at low collision energies due to the large exoergicity of the corresponding reactions.

The dominant reactions are believed to occur via a two-step mechanism as indicated in the schematic potential curve diagram shown in Fig. 10. Whereas the incoming channel is represented by a flat curve, the potential curves of the two dominant single- and double-electron-capture channels are shown as pure Coulombic curves. At a nuclear distance of about 6 a.u. (R_1) the first target electron is captured with high probability into the $4d$ and $4f$ orbitals in accordance with the measured single-capture spectrum. At nuclear distances below 4 a.u. (R_3) further crossings between the potential curves for single- and double-electron capture occur. In this case the second target electron is transferred into the $3d$ orbital of Ar^{6+}. The matrix element for a two-electron transition at R_2 is expected to be very small, as the energetic distance between the potential curves for single and double capture is very large at this internuclear distance [28–30].

IV. CROSS SECTIONS AND COLLISION FEATURES

In order to determine absolute cross sections (total and partial to individual substates), we first derive the emission cross sections $\sigma_{em}(\lambda)$ from the measured optical signals [31]. This quantity is written

$$\sigma_{em}(\lambda)=(4\pi/\Omega)S(\lambda)/(I/q)NLK(\lambda)\ , \tag{5}$$

where I is the ion beam current, q the incident ion charge, N the target number density, $S(\lambda)$ the measured signal, $K(\lambda)$ the spectrometer sensitivity, L the beam length viewed by the spectrometer, and Ω the solid angle.

The uncertainty of these cross sections is of the order of 30% and is basically due to the absolute calibration accuracy. Since in the Na-like spectrum there are no transitions of noticeable intensity originating from $n=5$ contributing by cascades to the population of the $n=4$, it is possible to express the capture cross section and thus compare the experimental values with theoretical predictions. Moreover, as discussed below, double capture practically does not interfere with single capture via autoionization into the $3p\,^2P^\circ_J$ or $3d\,^2D_J$ levels of Ar^{7+} (only a weak autoionization signal has been seen in the low-energy TES measurements). The end products of process (4) may decay to the Na-like ground state, but given the fact that the metastable fraction of the beam is below 5% and that a certain number of decay paths are autoionizing to the $2p^6\,^1S_0$ continuum, the contribution to the line intensities emitted after process (2) is assumed to be negligible.

A. Cross section for the excitation of Na-like Ar

The total single-electron-capture (SC) cross section may be written as follows:

$$\sigma_{SC}=\sigma_{em}(3s\,^2S_{1/2}\leftarrow 3p\,^2P^\circ_{1/2,3/2}) + \sigma_{em}(3s\,^2S_{1/2}\leftarrow 4p\,^2P^\circ)/BR\ . \tag{6}$$

The $3p\,^2P^\circ_J$ level is populated from all $4l\,^2L_J$ levels but the branching-ratio (BR) of the $4p\,^2P_J$ levels which decay to the ground state $3s\,^2S_{1/2}$. Given the transition probabilities and the branching ratio, the cross section for capture into different l orbitals of $n=4$ may be expressed as

$$\sigma_{4l}=\sigma_{em}(4l\rightarrow 3l')\left[\sum_{n'>l'} A_{4l'\rightarrow n'l'}\right]\Big/ A_{4l\rightarrow 3l'}\ . \tag{7}$$

At a collision energy of 2 keV/u we finally obtain for the total single-electron-capture cross section a value of

$$\sigma_{SC}=2.1\times 10^{-15}\ \text{cm}^2\ , \tag{8}$$

with the following sharing among the different $4l$ orbitals:

$$\begin{aligned}\sigma_{4s}&=2.1\times 10^{-16}\ \text{cm}^2\ \ (10\%)\ ,\\ \sigma_{4p}&=6.6\times 10^{-16}\ \text{cm}^2\ \ (32\%)\ ,\\ \sigma_{4d}&=9.1\times 10^{-16}\ \text{cm}^2\ \ (43\%)\ ,\\ \sigma_{4f}&=3.1\times 10^{-16}\ \text{cm}^2\ \ (14\%)\ .\end{aligned} \tag{9}$$

These values are in good agreement with theoretical predictions [23,24] and the total cross section also agrees well with previously measured ones (see Ref. [23] for previous references). The value measured by Druetta *et al.* [23] for the $n=4$ population is found to be somewhat smaller, even though the fractional sharing of the individual $n=4$ substates is similar. It should be noted that these authors mentioned some capture into $n=5$, as being also found in our low-energy TES spectra. However, in our vuv spectra, measured at 80 keV, no transitions from $n=5$ are observed. This finding agrees with recent observations by Boduch *et al.* [32]. They recorded optical spectra for $\Delta n=0$ transitions in the systems $Ar^{8+}+He$ and $Ar^{8+}+H_2$. Transitions for $n=5$ are only seen with the H_2 target, which is consistent with both our observation of the $n=4$ population and the theoretical result for the He target at this collision energy.

B. Double-capture cross section

Until recently the available spectroscopic data for Ar^{6+} were rather limited [8,12]. Our data [14–16] show that all $3l3l'\,^1L$ and $3l4l'\,^1L$ levels are lying below the first ionization limit of Mg-like Ar. This was also confirmed by Boduch *et al.* [32]. Since no theoretical treatment of the double capture is available, we use the reaction window-concept extensions [33,34] for predicting which are the most likely doubly excited ^1L levels. As in the $O^{8+}+He$ system, it appears that at 80 keV ($n=3,n'=3$) and ($n=3,n'=4$) are expected to be populated. Our TES measurements have shown that the latter configuration is populated preferably at low collision energies. All these highly doubly excited levels up to $3d4f$ lie just below the first ionization limit, thus their decay is fully radiative, whichever the populated levels are. A closer inspection of the level configuration shows that all the cascades finally feed the $2p^63s3p\,^1P^\circ_1$ level, the only level with a branching directly to the $2p^63s^2\,^1S_0$ level being the $2p^63s4p\,^1P^\circ_1$. Under these conditions, it is possible to write the total double-electron capture (DC) cross section as follows:

$$\sigma_{DC}=\sigma_{em}(2p^63s^2\,^1S_0\leftarrow 2p^63s3p\,^1P^\circ_1) + \sigma_{em}(2p^63s^2\,^1S_0\leftarrow 2p^63s4p\,^1P^\circ_1)\ . \tag{10}$$

Since the single-electron-capture cross section is known and since there is no strong interference between processes (2) and (3), the true double-capture cross section can be deduced. All line intensities given in Table I and II are normalized. Thus the ratio of the sum of intensities of transitions contributing to the double capture to the sum of the intensities of transitions contributing to the single-electron capture is a measure for the cross-section ratio. This ratio times the single-electron-capture cross sections gives the true double-electron-capture cross section. We obtain

$$\sigma_{DC}=5.12\times 10^{-16}\ \text{cm}^2\ , \tag{11}$$

with the sharing

$$\begin{aligned}\sigma_{DC}(n=3,n'=3)&=1\times 10^{-16}\ \text{cm}^2\ ,\\ \sigma_{DC}(n=3,n'=4)&=4.1\times 10^{-16}\ \text{cm}^2\ .\end{aligned} \tag{12}$$

The combination σ_{SC} and σ_{DC} may be considered as benchmarks for spectrometer calibration purposes, for example.

C. Capture cross section for the metastable projectile

If we compare SC by the metastable ion with the SC by the ground-state projectile, we note a great similarity to the capture level $n=4$. The sharing as understood from the Auger, the x-ray and the TES spectra shows a maximum population of the $2p^53s4d$ configuration (the ^2L

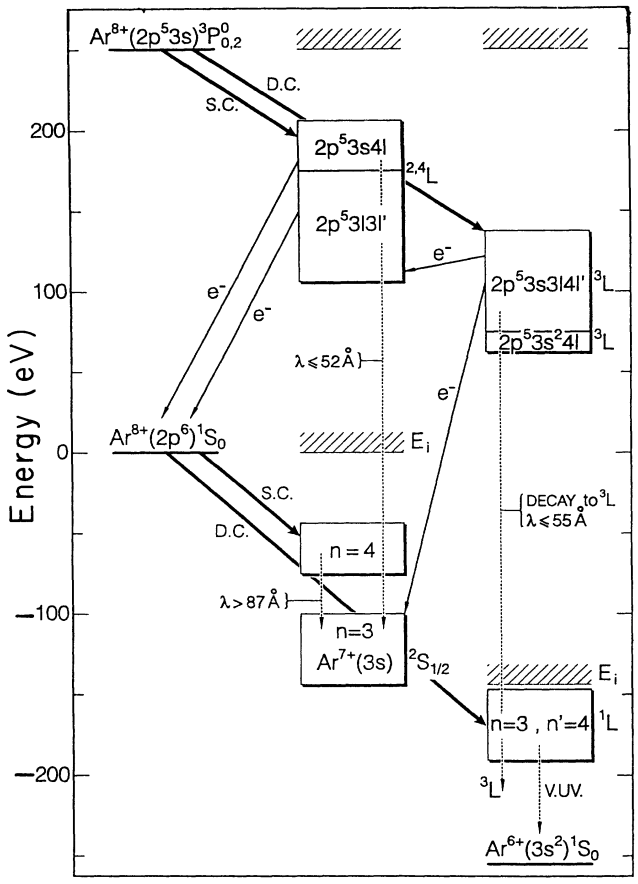

FIG. 11. Level diagram of the Ar^{8+} + He system. Left column: entrance channels; central column: single-capture exit channels to Na-like Ar; right column: double-capture exit channels to Mg-like Ar.

terms decay mostly via autoionization) very similar to the SC by the ground-state ion. On the basis of a Landau-Zener-type estimate, the total single-capture cross section would be the same as with the ground-state ion. All doubly excited levels below $2p^5 3s4l$ are in fact populated via cascades; the transfer excitation giving $2p^5 3p\ ^3Ln'l'$ would end in endothermic channels (the excitation energy $2p^5 3s\ ^3P$ to $2p^5 3p\ ^3L$ is of the order of 25 eV).

Assuming the same behavior for electron capture, whichever ion core is considered, the DC by the metastable ion would produce excited levels like $(2p^5 3s3l3l')^3L_J$ and $(2p^5 3s3l4l')^3L_J$, the transferred electron pair retaining its total spin and parity. These levels are not known. Considering calculated and measured energy gains for SC and DC by the ground-state ion, we can approximately locate the Mg-like triply excited Ar levels on an energy scale (see Fig. 11). The populated terms are ^1L for the ground-state projectile while ^3L results for the metastable ion. These triply excited levels would probably stabilize via autoionization to the closest continuum $2p^6 3l$ with emission of an electron (its kinetic energy is expected to be of the order of 235 eV). This could be the origin of a low-intensity peak around this value seen in the Auger spectrum [22].

Populating $2p^5 3s3d^2\ ^3L^\circ_J$ would probably open radiative channels; a first transition to $2p^6 3s3d\ ^3D_J$ would give a photon in the 3.7-nm range rapidly followed by a vuv transition $2p^6 3s3d\ ^3D_J \rightarrow 2p^6 3s3p\ ^3P^\circ_J$ (47.7 nm). Under the present conditions it seems difficult to reach directly for these transitions.

V. CONCLUSION

We have shown that SC and DC by Ar^{8+} ions in the ground state are populating levels under the first ionization limit in the Na- and Mg-like systems. Whereas SC populates dominantly the $4d$ level, DC produces with high probability the $3l4l'$ configurations, $3d4f$ and $3d4d$ being dominant at low collision energies. SC by the metastable ion $Ar^{8+*}(2p^5 3s)^3P_{0,2}$ populates core-excited Na-like Ar levels not well known before this work. [These levels are also populated in dielectronic recombination (DR).] A close inspection of the level characteristics shows that the ^4L_J levels are not systematically metastable against autoionization as in Li-like core-excited systems. It is important to differentiate between levels with ^1L and ^3L cores: they are different in energy and in their stabilization (radiation and autoionization). Since rate coefficients for DR are generally much smaller than those for charge transfer and since it is likely that DR may populate preferentially the ^1L core configurations, the necessity of knowing both appears. Both collision processes may well be cooperative in plasmas, e.g., for x-ray laser schemes or in Tokamaks when neutral hydrogen beams are used for heating and diagnostic purposes.

ACKNOWLEDGMENTS

The computations of one author (M.C.) were carried out on the NAS 9080 computer of the Centre de Calcul Electronique (CIRCE) France. The TES measurements have been performed at LAGRIPPA, a joint laboratory of the CEA and the CNRS; the assistance of A. Brenac, G. Lamboley, and Th. Lamy in providing the ion beam is gratefully acknowledged. Two of us (H.L. and B.A.H.) are grateful to the Deutsche Forschungsgemeinschaft for financial support. Two others (E.J.K. and S.B.) wish to thank NATO for a research grant (CRJ 8400682), which facilitated collaborative aspects of this work.

*Present address: Laboratoire de Spectroscopie Atomique et Ionique, Bâtiment 350, 91405 Orsay CEDEX, France.

[1] S. Bliman, D. Hitz, B. Jaquot, C. Harel, and A. Salin, J. Phys. B **16**, 2849 (1983).

[2] M. Boudjema, Ph.D. thesis, Université d'Alger, 1990.

[3] M. G. Suraud, J. J. Bonnet, M. Bonnefoy, M. Chassevent, A. Fleury, S. Bliman, S. Dousson, and D. Hitz, J. Phys. B **21**, 1219 (1988).

[4] L. Guillemot, P. Roncin, M. N. Gaboriaud, M. Barat, H. Laurent, S. Bliman, M. G. Suraud, D. Hitz, J. J. Bonnet,

M. Bonnefoy, M. Chassevent, and A. Fleury, J. Phys. B **23**, 335 (1990).
[5] S. Bliman, M. G. Suraud, D. Hitz, J. E. Rubensson, J. Nordgren, M. Cornille, P. Indelicato, and E. J. Knystautas, J. Phys. B **22**, 3647 (1989).
[6] E. Hinnov and F. Hofman, J. Opt. Soc. Am. **53**, 1259 (1963).
[7] J. Nordgren and R. Nyholm, Nucl. Instrum. Methods A **246**, 314 (1986).
[8] R. L. Kelly, J. Phys. Chem. Ref. Data **16**, Parts 1 and 3 (1987).
[9] B. A. Huber, Comments At. Mol. Phys. **21**, 15 (1987).
[10] H. Lebius and B. A. Huber, Z. Phys. D **21**, S271 (1991).
[11] H. Lebius, Ph.D. thesis, Ruhr-Universität Bochum, 1991.
[12] S. Bashkin and J. O. Stoner, Jr., *Atomic Energy Levels and Grotrian Diagrams* (North-Holland, New York, 1978), Vol. 2.
[13] A. Lindgard and S. E. Nielsen, At. Data Nucl. Data Tables **19**, 537 (1977).
[14] S. Bliman, P. Indelicato, D. Hitz, P. Marseille, and J. P. Desclaux, J. Phys. B **22**, 2741 (1989).
[15] P. Marseille, S. Bliman, J. P. Desclaux, S. Dousson, and D. Hitz, J. Phys. B **20**, 5127 (1987).
[16] P. Marseille, S. Bliman, P. Indelicato, and D. Hitz, J. Phys. B **20**, L423 (1987).
[17] W. Eissner and H. Nussbaumer, Comput. Phys. Commun. **8**, 270 (1974).
[18] W. Eissner and M. J. Seaton, J. Phys. B **5**, 2188 (1972).
[19] M. J. Seaton, J. Phys. B **7**, 1817 (1974).
[20] TFR Group, J. Dubau, and M. Loulergue, J. Phys. B **15**, 1907 (1981).
[21] E. Luc-Koenig and J. Bauche, J. Phys. B **23**, 1763 (1990).
[22] E. M. Mack, Ph.D. thesis, University of Utrecht, 1997.
[23] M. Druetta, S. Martin, T. Bouchama, C. Harel, and H. Jouin, Phys. Rev. A **36**, 3071 (1987).
[24] R. McCarroll, in *Recent Studies in Atomic and Molecular Processes,* edited by A. E. Kingston (Plenum, New York, 1987), p. 113.
[25] M. Barat and P. Roncin (private communication).
[26] M. Kimura and R. E. Olson, Phys. Rev. A **31**, 489 (1985).
[27] J. P. Desclaux, Comput. Phys. Commun. **9**, 31 (1974).
[28] P. Roncin, M. Barat, and H. Laurent, Europhys. Lett. **2**, 371 (1986).
[29] H. Laurent, M. Barat, M. N. Gaboriaud, L. Guillemot, and P. Roncin, J. Phys. B **20**, 6581 (1987).
[30] H. R. Koslowski and B. A. Huber, J. Phys. B **22**, 2255 (1989).
[31] K. Kadota, D. Dijkkamp, R. L. van der Woude, A de Boer, Pan Guang Yan, and F. J. de Heer, J. Phys. B **15**, 3275 (1982).
[32] P. Boduch, M. Chantepie, D. Hennecart, X. Husson, H. Kucal, D. Lecler, and I. Lestevenvaise, J. Phys. B **22**, L377 (1989).
[33] A. Barany, G. Astner, H. Cederquist, H. Danared, S. Huldt, P. Hvelplund, A. Johnson, H. Knudsen, L. Liljeby, and K. G. Rensfelt, Nucl. Instrum. Methods **B 9**, 397 (1985).
[34] A. Niehaus, J. Phys. B **19**, 2925 (1986).